Model-Free Energy-Based Friction Compensation for Industrial Collaborative Robots as Haptic Displays

Huseyin Tugcan Dinc, *Graduate Student Member, IEEE*,
Joong-Ku Lee, *Graduate Student Member, IEEE*, and Jee-Hwan Ryu, *Senior Member, IEEE*

***Abstract*—Collaborative robots are a promising alternative to traditional haptic displays due to their expansive workspaces, ability to generate substantial forces, and cost-effectiveness. However, they have higher levels of friction compared to conventional haptic displays, which negatively impact the precise movement and accuracy of haptic feedback, potentially causing operator fatigue. This article proposes a novel model-free, energy-based approach for estimating and compensating the friction coefficient. Our approach calculates the time-varying impact of frictional forces during an energy cycle, defined as the period between two consecutive zero crossings of the system's kinetic energy, based on the energy dissipated by friction. This approach directly estimates the friction coefficients, based on the chosen friction model, without requiring any prior system model information or tuning parameters. The effectiveness of our approach is demonstrated through single and multi-degree-of-freedom human interaction experiments using a Franka Emika Panda robot. The results indicate that the proposed approach outperforms state-of-the-art friction compensation methods.**

***Index Terms*—Adaptive friction compensation, collaborative robots, conservation of energy.**

I. Introduction

COLLABORATIVE robots have the potential to serve as effective haptic displays owing to their workspace being comparable to that of a human arm, their capacity to generate substantial force, and their cost-effectiveness [1]. Given the current trend toward increasing the affordability and accessibility of collaborative robots, they present a promising and versatile option as alternative to conventional haptic displays for various applications [2], [3]. Furthermore, precise force control capabilities further enhance their utility and render them a compelling substitute for conventional haptic displays.

Fig. 1. Bimanual haptic display with Franka Emika Panda robot arms.

As illustrated in Fig. 1, collaborative robot arms are recently employed as haptic displays, especially for tasks requiring a wide range of human arm movements. In a study [4], a lightweight robot invented by the German Aerospace Center (DLR) was employed as a bimanual haptic display to interact with virtual environments and remotely control the upper body of Justin [5]. Another intriguing example of an industrial collaborative robot utilized as a haptic display was presented at the ANA Avatar XPRIZE challenge [6]. The Nimbro team employed two Franka Emika collaborative robots as bimanual haptic displays that emerged victorious in the competition.

However, the utilization of industrial collaborative robots as haptic displays faces limitations, notably their relatively higher friction levels than those of conventional haptic displays. This increased friction results in decreased accuracy and precision of the haptic feedback delivered by these robots, thereby exacerbating operator fatigue in scenarios involving prolonged usage [7]. This challenge is particularly prominent when impedance-type haptic displays are deployed and the application demands high accuracy and precision.

Manuscript received 3 December 2023; revised 4 April 2024; accepted 27 May 2024. This work was supported in part by the Ministry of Trade, Industry & Energy (MOTIE, Korea), through Robot Industry Core Technology Development Program (Development of shared autonomy control framework and AI-based application technology for enhancing tasks of hyper realistic telepresence robots in unstructured environment) under Grant 20023294 and in part by the National Research Foundation of Korea under Grant NRF-2020R1A2C200416915. *(Huseyin Tugcan Dinc and Joong-Ku Lee contributed equally to this work.) (Corresponding author: Jee-Hwan Ryu.)*

Huseyin Tugcan Dinc is with the Robotics Program, Korea Advanced Institute of Science and Technology, Daejeon 34141, South Korea (e-mail: htdinc@kaist.ac.kr).

Joong-Ku Lee and Jee-Hwan Ryu are with the Department of Civil and Environmental Engineering, Korea Advanced Institute of Science and Technology, Daejeon 34141, South Korea (e-mail: iamjoong9@kaist.ac.kr; jhryu@kaist.ac.kr).

Color versions of one or more figures in this article are available at https://doi.org/10.1109/TMECH.2024.3410330.

Digital Object Identifier 10.1109/TMECH.2024.3410330

Friction compensation has been extensively studied in robotics [8]. Friction compensation methods can be broadly classified as model-based and model-free methods [9], [10]. Model-based methods utilize system dynamic parameters to estimate frictional effects, while model-free methods do not require any system parameter to estimate frictional effects. Both model-based and model-free friction compensation methods can be implemented offline and online (adaptive) manner [11]. Offline methods make use of pre-estimated fixed parameters, whereas online methods employ real-time estimation techniques for friction compensation [12].

Offline friction compensation techniques often exhibit limited performance due to the dynamic and time-varying nature of friction, particularly in complex systems with high nonlinearities. In a previous study [13], an offline model-based friction estimation was conducted on the Franka Emika Panda collaborative robot using a penalty-based optimization technique with a system model. Another study [14] explored the impact of load and position dependencies on frictional effects. In this work, the authors introduced a novel friction model based on the system's dynamics to account for these dependencies. In addition, the influence of temperature on friction in industrial robots was investigated in [15]. They incorporated temperature as a parameter in the friction model to enhance the accuracy of friction estimation.

Due to time-varying friction, online methods generally outperform offline methods. However, existing online friction compensation algorithms usually rely on a system model. In a study [16], a disturbance observer-based (DOB) friction compensation was presented. This approach used an observer with a dynamic model of the robot joint to estimate friction. Another approach used joint torque feedback for motor inertia reshaping and friction reduction [17]. In this case, a system model for the motor system was also necessary. Recently, passivity-based adaptive friction compensation for underactuated mechanical systems has been explored [18]. Although this approach does not require prior knowledge of the friction parameters, it involves solving partial differential equations, presenting challenges for systems with higher degrees of freedom (DoF).

This study introduces a model-free, energy-based adaptive friction compensation technique that differs from traditional methods. By applying the conservation of energy law, it calculates the time-varying impact of frictional torques during an energy cycle, defined as the period between two consecutive zero crossings of the system's kinetic energy. The method offers two key advantages: independence from the robot system's model information and simplicity in its online application. It estimates friction effects based on energy levels during human–robot interaction, eliminating the need for system model identification. Furthermore, our approach directly estimates friction coefficients for the given friction model, requiring no system related tuning parameters. Experimental validation was conducted using a Franka Emika Panda robot for both single-DoF and multi-DoF interactions. The results demonstrate its superior performance compared to other friction compensation methods, including model-based [13], DOB-based [16], and output torque regulation [17] approaches.

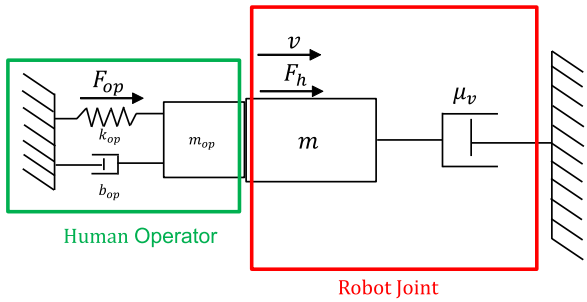

Fig. 2. Mechanical representation of a single-DoF robot joint interacting with a human operator without friction compensation. μ_v denotes the friction coefficient of the robot joint.

The rest of this article is organized as follows. Section II presents an energy-based analysis of friction based on the principle of energy conservation and models the energy exchange during interactions. Section III introduces energy-based friction estimation, and Section IV reports on the stability analysis performed for the proposed method. Section V presents the experimental results for both single-DoF and multi-DoF cases and a comparison is presented between the proposed and other friction compensation methods. Finally, Section VI concludes this article.

II. Modeling of Energy Exchange During Physical Human–Robot Interaction (pHRI)

This section elucidates the fundamental concept of the proposed energy-based friction compensation approach by analyzing the energy exchange that occurs during pHRI between a human operator and a robot joint.

Fig. 2 presents a simplified physical interpretation of a single-DoF robot joint that interacts with a human operator without friction compensation. To simplify the analysis and broaden the applicability of our approach, a rigid joint model is used in this study, although a flexible joint model may provide more accurate descriptions for certain robotic systems. The human operator is modeled as a mass–spring–damper system (m_{op}, k_{op}, and b_{op}), and applies a human torque (F_h) to the robot joint that comprises a single mass (m) and inherent viscous friction (μ_v), by stimulating the muscle force (F_{op}). Consequently, the robot joint moves at the same velocity (v) as the human operator. In this section, the friction of a robot joint is modeled as viscous friction to yield a more comprehensive explanation. Therefore, the friction torque is modeled as

$$F_f = -\mu_v v. \tag{1}$$

Nonetheless, friction can be represented by other conventional friction models [8], such as the Coulomb and combined (Coulomb + viscous) friction models, which relate friction to the steady-state velocity of a system.

The human torque (F_h) is applied to the robot joint, and the resultant interaction torque is measured by the joint torque sensor, defined as F_m in this study. In practice, the joint torque

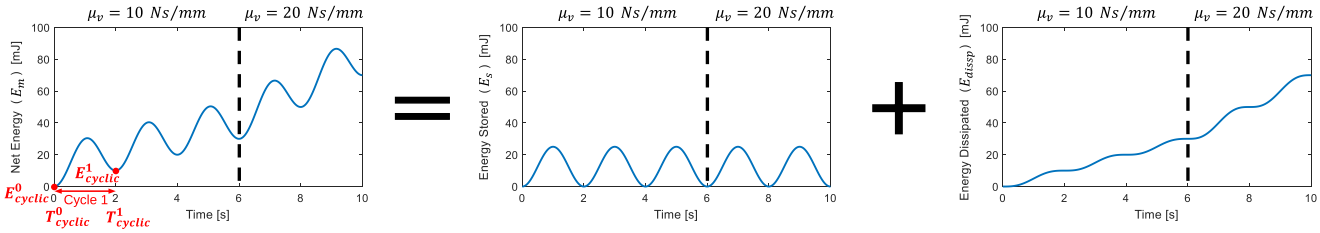

Fig. 3. Net energy input during human–robot joint interaction, consisting of oscillating kinetic energy and monotonically increasing dissipative energy. The energy conservation law relates the net energy input to the stored kinetic energy and dissipated energy by joint friction.

measurements encompass all external and internal torques acting on the joint, such as interaction torque and compensation torques. The measured interaction torque (F_m), thus, represents the resultant driving torque of the joint before it is affected by frictional torques. Consequently, the energy input introduced by the human operator can be calculated using power conjugates pairs, specifically the measured interaction torque (F_m) and velocity (v), for a given time (T) as

$$E_m(T) = \Delta T \sum_{t=0}^{T} F_m(t)v(t) \tag{2}$$

where F_m represents the interaction torque measured by the joint torque sensor, v denotes joint velocity, and ΔT represents the sampling period. Reducing the sampling period (ΔT) tends to enhance system performance at the expense of increased computational costs. In this work, we selected a 1 ms sampling period to provide sufficient processing capacity and meet real-time deadlines.

Based on the energy conservation law, the net energy input to the robot joint from the human operator (E_m) is partially stored at the robot joint, and the remaining energy is dissipated, thereby satisfying the energy conservation law as follows:

$$E_m(T) = E_s(T) + E_{\text{dissp}}(T) \tag{3}$$

where $E_s(T)$ is the stored energy in the joint mass m and $E_{\text{dissp}}(T)$ is the dissipated energy attributed to the internal friction of the joint. Under the assumption of perfect gravity compensation and, hence, no gravitational potential energy of the joint mass, the stored energy (E_s) can be calculated using the basic kinetic energy equation as follows:

$$E_s(T) = \frac{1}{2}mv(T)^2 \tag{4}$$

and given the friction coefficient (μ_v) and flow (v), E_{dissp} can be computed as

$$E_{\text{dissp}}(T) = \Delta T \sum_{t=0}^{T} \mu_v v(t)^2. \tag{5}$$

Therefore, under ideal conditions, the energy conservation law (3) can be represented in a discrete domain as follows:

$$\Delta T \sum_{t=0}^{T} F_m(t)v(t) = \frac{1}{2}mv(T)^2 + \Delta T \sum_{t=0}^{T} \mu_v v(t)^2. \tag{6}$$

A simulation was conducted to demonstrate the typical energy-exchange behavior during pHRI; we assumed that the human operator interacted sinusoidally with the robot joint. The simulation results, as plotted in Fig. 3, indicate that the net energy input to the robot comprises two components: oscillating kinetic energy (E_s) and monotonically increasing dissipative energy (E_{dissp}). The bumpy shapes of the energy curve (E_m) can be interpreted as the kinetic energy storage and release characteristics of the joint mass, whereas the increasing local minimum points correspond to the energy dissipated by the joint friction.

III. Energy-Based Friction Estimation

Considering the system presented in Fig. 2 and the corresponding energy equation (6), the inherent viscous friction coefficient (μ_v) can be inversely estimated if the net energy input and the kinetic energy are known. In general, the net energy input (E_m) can be numerically calculated by integrating the measured interaction torque and velocity. However, accurately estimating the kinetic energy (E_s) can be difficult because the joint mass (m) is often unknown.

When the kinetic energy of the system reduces to zero (i.e., the robot joint velocity $v = 0$), the relationship between the net energy input and the energy dissipated by viscous friction becomes apparent. Consequently, the viscous friction coefficient can be estimated without prior knowledge of the joint mass. To this end, the nth instance when the robot joint velocity reduces to zero is defined as T^n_{cyclic}, and the corresponding net energy-input values are defined as E^n_{cyclic}. The period between T^{n-1}_{cyclic} and T^n_{cyclic} is defined as the nth energy cycle, starting when the joint velocity becomes a nonzero value and terminating upon attaining a zero value. These variables are illustrated in Fig. 3 for a clear representation.

As the kinetic energy at the end of each cycle eventually becomes zero, a modified version of equation (6) is rendered feasible by setting the kinetic energy to zero. This allows for the establishment of a relationship between the net energy input to the robot joint from the previous cyclic period T^{n-1}_{cyclic} to the current cyclic period T^n_{cyclic} and the energy dissipated by viscous friction; the relationship is as follows:

$$\Delta T \sum_{t=T^{n-1}_{\text{cyclic}}}^{T^n_{\text{cyclic}}} F_m(t)v(t) = E^n_{\text{cyclic}} - E^{n-1}_{\text{cyclic}} = \Delta T \sum_{t=T^{n-1}_{\text{cyclic}}}^{T^n_{\text{cyclic}}} \mu_v v(t)^2. \tag{7}$$

Therefore, after the cycle is terminated, the friction coefficient of the robot joint can be inversely estimated at each end of the

cycle as follows:

$$\mu_v^{\text{est}} := \frac{E_{\text{cyclic}}^n - E_{\text{cyclic}}^{n-1}}{\Delta T \sum_{t=T_{\text{cyclic}}^{n-1}}^{T_{\text{cyclic}}^n} v(t)^2}. \tag{8}$$

The estimated friction coefficient can be subsequently employed as the coefficient of the friction compensator

$$F_{\text{comp}} = -\mu_v^{\text{comp}} v \tag{9}$$

where $\mu_v^{\text{comp}} = -\mu_v^{\text{est}}$ to compensate for the inherent viscous friction in the robot joint.

Upon implementing the friction compensator in the system, the friction-coefficient estimation process must be modified in subsequent cycles. This is because the friction compensator introduces an additional component that can affect the net energy input to the system. The net energy input for each cycle must be adjusted to account for the impact of the friction compensator on the system, and the resulting modified net energy input is obtained as

$$E_{\text{cyclic}}^n - E_{\text{cyclic}}^{n-1} - \Delta T \sum_{t=T_{\text{cyclic}}^{n-1}}^{T_{\text{cyclic}}^n} \mu_v^{\text{comp}} v(t)^2 = \Delta T \sum_{t=T_{\text{cyclic}}^{n-1}}^{T_{\text{cyclic}}^n} \mu_v v(t)^2 \tag{10}$$

where μ_v^{comp} denotes the coefficient of the friction compensator applied during the nth cycle. Accordingly, the friction coefficient estimation equation considering previous energy cycle's friction compensator can be written as

$$\mu_v^{\text{est}} := -\mu_v^{\text{comp}} + \frac{E_{\text{cyclic}}^n - E_{\text{cyclic}}^{n-1}}{\Delta T \sum_{t=T_{\text{cyclic}}^{n-1}}^{T_{\text{cyclic}}^n} v(t)^2}. \tag{11}$$

Hence, the coefficient of friction compensator μ_v^{comp} for the next energy cycle is updated to $-\mu_v^{\text{est}}$. This process is repeated for each subsequent energy cycle, thereby facilitating the continuous estimation and updating of the friction compensation coefficient during the interaction. Notably, the method presented in this study is capable of handling time-varying friction, which may be influenced by various factors such as operating time, temperature, pressure, and other internal and external conditions.

To evaluate the feasibility of the proposed model-free, energy-based adaptive friction compensation method, we conducted a simulation using the same environment as that presented in Section II. The mechanical and electrical analogies of a single-DoF robot joint equipped with a friction compensator interacting with the human operator are illustrated in Fig. 4 and the comprehensive control scheme, featuring the proposed friction compensator, is visually represented in Fig. 5. The measured interaction torque (F_m) encompasses all external torques (human applied torque F_h and gravity torque F_g) and internal torques (gravity compensation torque $F_{g_{\text{comp}}}$ and friction compensation torque F_{comp}) applied on the robot joint. These torque act upon the system in conjunction with the friction torque F_f, resulting in a velocity v. Joint torque sensors measure the resultant torque F_m, which is subsequently utilized to compute the estimated friction coefficient, denoted as μ_{est}. These estimated friction coefficients are both transmitted to the friction compensator and updated after each energy cycle.

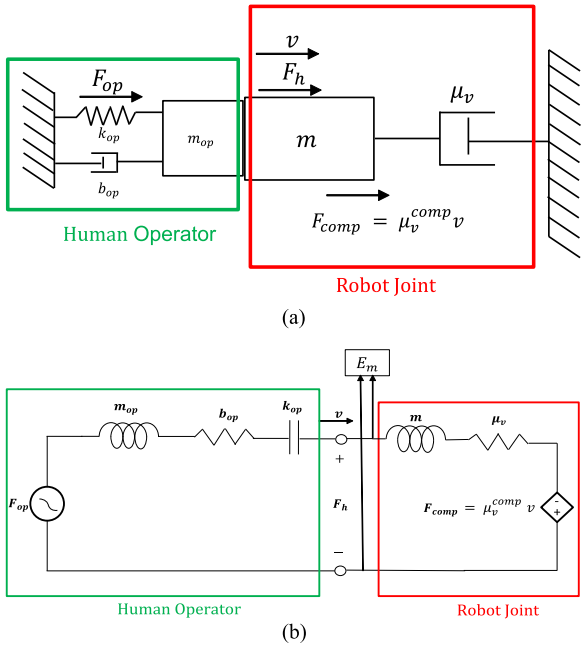

Fig. 4. (a) Mechanical and (b) electrical representation of a single-DoF robot jointly interacting with a human operator with friction compensation.

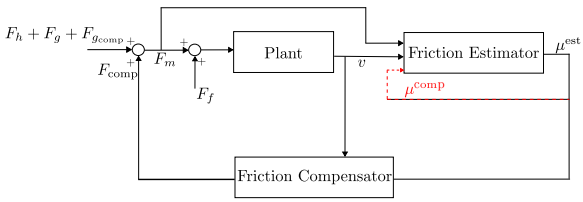

Fig. 5. Control scheme of the proposed energy-based friction compensation approach.

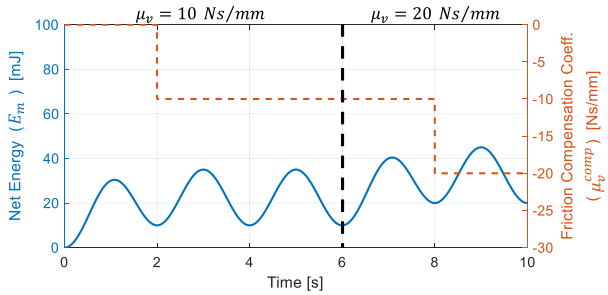

Fig. 6. Simulation of mass-viscous friction system with adaptive friction compensator with different friction coefficients: 0–6 s μ_v = 10 Ns/mm, 6–10 s μ_v = 20 Ns/mm.

The net energy input (E_m) and estimated friction coefficient (μ_v) obtained using the proposed method are shown in Fig. 6. In the first cycle (duration: $(0-2)$ s), energy dissipation is allowed because the proposed method requires at least one cycle to estimate a single friction coefficient. After the first cycle, the friction coefficient is estimated based on the energy difference, and the coefficient of the viscous friction compensator is updated

to 10 Ns/mm, which is identical to the inherent viscous friction coefficient of the joint assigned for the simulation. Subsequently, energy dissipation does not occur during the second and third cycles because the inherent joint friction is perfectly compensated by the proposed method. Even when the friction coefficient of the joint suddenly rises to 20 Ns/mm at 6 s, the proposed method can accurately estimate and further compensate for the change in the friction coefficient of the robot joint after the fourth energy cycle is concluded. This shows the adaptability of the proposed friction compensation approach in the presence of time-varying frictional effect.

The selection of a suitable friction model is essential for achieving high-performance outcomes with the proposed method. Thus far, we introduced our approach by employing a viscous friction model. Nonetheless, as mentioned before, our approach can be extended to any other friction model that represents the friction force as a function of steady-state velocity, such as the Coulomb and combined friction models. When the system friction model is considered as a Coulomb friction model, the frictional torque is formulated as follows:

$$F_f = -\mu_c \text{sgn}(v) \tag{12}$$

where μ_c is the coefficient of the Coulomb friction model. Thus, similar to (10), the net energy input for each cycle can be analyzed as follows:

$$E^n_{\text{cyclic}} - E^{n-1}_{\text{cyclic}} - \Delta T \sum_{t=T^{n-1}_{\text{cyclic}}}^{T^n_{\text{cyclic}}} \mu_c^{\text{comp}} \text{sgn}\left(v(t)\right) \cdot v(t)$$

$$= \Delta T \sum_{t=T^{n-1}_{\text{cyclic}}}^{T^n_{\text{cyclic}}} \mu_c \text{sgn}\left(v(t)\right) \cdot v(t) \tag{13}$$

and finally, the friction coefficient estimation equation can be represented as

$$\mu_c^{\text{est}} := -\mu_c^{\text{comp}} + \frac{E^n_{\text{cyclic}} - E^{n-1}_{\text{cyclic}}}{\Delta T \sum_{t=T^{n-1}_{\text{cyclic}}}^{T^n_{\text{cyclic}}} \text{sgn}(v(t)) \cdot v(t)}. \tag{14}$$

Furthermore, if the friction model is selected as a combined friction model, the friction torque can be represented as

$$F_f = -\mu_c \text{sgn}(v) - \mu_v v \tag{15}$$

where μ_c and μ_v are the coefficients of the Coulomb and viscous friction, respectively. In this case, the net energy input for each cycle can be analyzed as

$$E^n_{\text{cyclic}} - E^{n-1}_{\text{cyclic}} - \Delta T \sum_{t=T^{n-1}_{\text{cyclic}}}^{T^n_{\text{cyclic}}} \left\{\mu_c^{\text{comp}} \text{sgn}(v(t)) \cdot v(t) + \mu_v^{\text{comp}} v(t)^2\right\}$$

$$= \Delta T \sum_{t=T^{n-1}_{\text{cyclic}}}^{T^n_{\text{cyclic}}} \left\{\mu_c \text{sgn}(v(t)) \cdot v(t) + \mu_v v(t)^2\right\}. \tag{16}$$

Estimating the friction coefficients of the combined friction model is inherently nondeterministic within a single cycle due to the presence of two unknown variables, denoted as μ_v and μ_c. To address this challenge, we employed a strategy that leverages two or more energy cycles to determine the optimal values of μ_v and μ_c. In other words, we acquired two or more linear equations of (16) and subsequently solved a system of linear equations to derive the friction coefficient values. It is important to note that our approach assumes the linear independence of these equations, as encountering identical velocity and torque profiles during pHRI cycles is unlikely. When we express the left side of (16) as E^n_{net}, we can rewrite it as follows:

$$E^n_{\text{net}} = \mu_c \cdot \Delta T \sum_{t=T^{n-1}_{\text{cyclic}}}^{T^n_{\text{cyclic}}} \text{sgn}(v(t)) \cdot v(t) + \mu_v \cdot \Delta T \sum_{t=T^{n-1}_{\text{cyclic}}}^{T^n_{\text{cyclic}}} v(t)^2. \tag{17}$$

Now, when considering the prior k number of cycles from the most recent nth cycle, the equation can be represented in matrix form as

$$\begin{bmatrix} E^{n-k+1}_{\text{net}} \\ \vdots \\ E^n_{\text{net}} \end{bmatrix} = \begin{bmatrix} \Delta T \sum_{t=T^{n-k}_{\text{cyclic}}}^{T^{n-k+1}_{\text{cyclic}}} \text{sgn}(v(t)) \cdot v(t) & \Delta T \sum_{t=T^{n-k}_{\text{cyclic}}}^{T^{n-k+1}_{\text{cyclic}}} v(t)^2 \\ \vdots & \\ \Delta T \sum_{t=T^{n-1}_{\text{cyclic}}}^{T^n_{\text{cyclic}}} \text{sgn}(v(t)) \cdot v(t) & \Delta T \sum_{t=T^{n-1}_{\text{cyclic}}}^{T^n_{\text{cyclic}}} v(t)^2 \end{bmatrix} \cdot \begin{bmatrix} \mu_c \\ \mu_v \end{bmatrix} \tag{18}$$

in the condition where $n \geq 2$, $k \geq 2$, and $n \geq k$. This overdetermined linear equation, expressed as $b = Ax$, can be solved using the Moore–Penrose pseudoinverse method. Specifically, the pseudoinverse A^+ is computed as

$$A^+ = A^T (A A^T)^{-1} \tag{19}$$

and as a result, the variables μ_v and μ_c are inversely estimated as

$$\begin{bmatrix} \mu_c \\ \mu_v \end{bmatrix} = \begin{bmatrix} \Delta T \sum_{t=T^{n-k}_{\text{cyclic}}}^{T^{n-k+1}_{\text{cyclic}}} \text{sgn}(v(t)) \cdot v(t) & \Delta T \sum_{t=T^{n-k}_{\text{cyclic}}}^{T^{n-k+1}_{\text{cyclic}}} v(t)^2 \\ \vdots & \\ \Delta T \sum_{t=T^{n-1}_{\text{cyclic}}}^{T^n_{\text{cyclic}}} \text{sgn}(v(t)) \cdot v(t) & \Delta T \sum_{t=T^{n-1}_{\text{cyclic}}}^{T^n_{\text{cyclic}}} v(t)^2 \end{bmatrix}^+ \cdot \begin{bmatrix} E^{n-k+1}_{\text{net}} \\ \vdots \\ E^n_{\text{net}} \end{bmatrix}. \tag{20}$$

It is important to highlight that this algorithm requires at least two consecutive cycles to estimate the friction coefficients. However, based on the author's experience, utilizing a small number of cycles may lead to inaccurate estimations of friction coefficients, unless the data from each cycle exhibit distinct energy and velocity levels. Consequently, the number of cycles used for

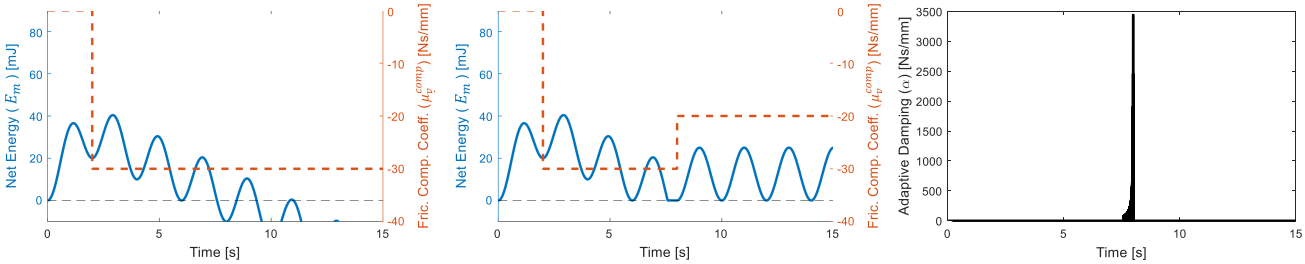

Fig. 7. (a) Simulation result showing the energy when friction is overcompensated. The system viscous friction coefficient is set to 20 Ns/mm and overcompensated with 30 Ns/mm. (b) Activation of the passivity controller to the friction overcompensated system. (c) Adaptive damping applied to the system. The passivity controller is activated in fourth cycle to passivate the system and the friction compensation coefficient is updated based on the dissipated energy by the passivity controller.

estimation (k) is considered a key parameter in this algorithm. While a larger number of cycles tends to yield more stable results, it could also slow down the adaptation to the system's true time-varying friction coefficients.

IV. Stability Analysis of the Proposed Friction Compensator

In the pHRI, the stability of the system is a critical factor for ensuring safe and reliable interactions. Among the various methods used for stability analysis, passivity has been widely utilized in pHRI systems [19]. A system that dissipates energy, or at least does not generate energy, is considered passive and, hence, stable because passivity is a subset of stability. Conversely, a system that generates energy is considered active and potentially unstable. The proposed energy-based friction compensation approach can act as an active component. Therefore, identifying and passivating the proposed friction compensator is necessary for stable interaction.

The passivity of the robot joint incorporating the proposed friction compensator over the one-port network [see Fig. 4(b)] is identified by the following passivity rule:

$$\int_0^t f(\tau)v(\tau)d\tau + E(0) \geq 0. \tag{21}$$

Herein, $E(0)$ is the initial stored energy and f and v are the effort source and flow, respectively. In the discrete system, the energy over time can be calculated using the (2). If the system satisfies the passivity rule (21) all the time, the system dissipates energy and is, thus, passive.

Upon implementing the proposed friction compensation method, three distinct scenarios may arise based on the level of compensation provided: undercompensation, perfect compensation, and overcompensation. In the case of undercompensation, the residual friction in the system dissipates energy, resulting in the system being passive. When friction is perfectly compensated, no energy is produced or dissipated, resulting in a marginally passive system. However, in instances where friction is overcompensated [see Fig. 7(a)], the system may generate excessive energy, potentially violating the passivity rule (21) and leading to instability. To mitigate this concern, we implemented the time-domain passivity approach (TDPA) [20] to preserve system passivity by ensuring that energy remains positive. While this approach might entail some performance tradeoffs, it effectively guarantees the passivity and stability of the system.

The necessary adaptive damping value that should be injected by the TDPA to satisfy (21) can be calculated with

$$\alpha := \begin{cases} -\frac{E_m}{v^2 \Delta T} & E_m < 0 \\ 0 & E_m \geq 0 \end{cases} \tag{22}$$

where E_m is the net energy input introduced to the robot, which is calculated using (2). Based on the observed energy, the passivity controller should be applied to the friction compensation torque F_{comp} as

$$F_{\text{comp}} = \mu_v^{\text{comp}} v + \alpha v. \tag{23}$$

When the energy cycle includes a nonzero α and the passivity controller is activated, the dissipated energy by the passivity controller in the nth energy cycle (E_{TDPA}^n) can be calculated using the equation

$$E_{\text{TDPA}}^n = \Delta T \sum_{t=T_{\text{cyclic}}^{n-1}}^{T_{\text{cyclic}}^n} \alpha(t) v(t)^2. \tag{24}$$

Since the passivity controller is activated in the nth cycle, E_{cyclic}^n is zero, but E_{cyclic}^{n-1} can be nonzero value. Therefore, the total energy generated in the nth cycle can be represented as $E_{\text{cyclic}}^{n-1} + E_{\text{TDPA}}^n$. The friction coefficient estimation equation, considering the dissipated energy by the passivity controller, is given by

$$\mu_v^{\text{est}} := -\mu_v^{\text{comp}} + \frac{-E_{\text{TDPA}}^n - E_{\text{cyclic}}^{n-1}}{\Delta T \sum_{t=T_{\text{cyclic}}^{n-1}}^{T_{\text{cyclic}}^n} v(t)^2}. \tag{25}$$

This method enables the update of the friction coefficient even when the passivity controller is activated, as illustrated in Fig. 7(b), and adaptive damping injected by TDPA is shown in Fig. 7(c). The integration of a passivity controller within our proposed friction compensation approach guarantees the system's passivity, thereby mitigating any potential instabilities that may arise from the misestimation of the friction coefficients. It is worth noting that this method can be easily applied to the

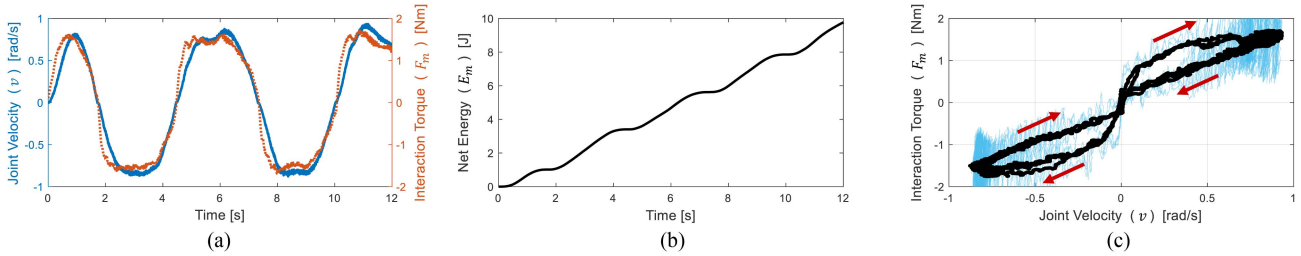

Fig. 8. Experimental data without any friction compensation on a single joint of the robot arm. (a) Joint velocity and interaction torque of the robot joint interacting with the human operator. (b) Net energy input from the human operator to the robot joint. (c) Joint velocity versus interaction torque curve with raw (blue) and filtered (black) values. The red arrows show the direction over time.

Coulomb and combined friction estimation process, by substituting E^n_{cyclic} to E^n_{TDPA} in (14) and (16).

V. Experimental Study

To validate the feasibility of our model-free energy-based friction compensation approach in a real robotic system, we conducted experiments using a Franka Emika Panda robot arm. Three sets of experiments were conducted to validate the effectiveness of our proposed approach. In the first set of experiments, we applied the proposed approach to a single joint of a robotic arm to assess its feasibility. Specifically, we utilized the first joint of the panda robot arm. Next, we extended our approach to the whole 7 joints of a robot arm to test its validity in multi-DoF systems. Finally, we conducted a comparative study between our proposed approach and other friction compensation methods to investigate its performance. For these experiments, a combined friction model was used, and the number of cycles for estimation (k) was set as two.

In the experiments, human operators perform spontaneous movements without predefined interaction trajectories. The internal controller perfectly compensates for gravity torque, allowing for the interaction torque from the human operator to be utilized in energy calculation. It is important to note that the energy cycle detection algorithm employs the joint's filtered velocity for cycle detection. Specifically, an energy cycle is identified only when the filtered velocity completely exceeds the initiation velocity threshold and subsequently descends below the termination velocity threshold. To ensure accurate detection of energy cycles, especially at low joint velocities, the initiation velocity threshold is deliberately set higher than the termination velocity threshold. For this study, these thresholds were experimentally determined to be 0.2 rad/s for initiation and 0.05 rad/s for termination. However, these threshold values might need adjustment depending on the robotic system used in human–robot interactions, necessitating an experimental tuning process for each system. It is worth noting that a too small velocity threshold could result in false detection of energy cycles, whereas a too high threshold might miss some energy cycles.

A. Experiment With a Single Robot Joint

First, an experiment was conducted on a single joint of a robot arm without friction compensation to investigate the energy behavior of a real robot system. The joint velocity and measured interaction torque, denoted as v and F_m in Fig. 2, respectively, are presented in Fig. 8(a). The results demonstrate an oscillatory but increasing behavior of the net energy input from the human operator to the robot, as plotted in Fig. 8(b). This behavior is attributed to intrinsic joint friction, which dissipates the energy introduced by the human operator. The joint velocity versus interaction torque curve is presented in Fig. 8(c). The joint velocity versus interaction torque curve of the real robot joint without friction compensation exhibits a profile similar to the dashed line in Fig. 9, which depicts the simulated result when the inherent combined friction is not compensated. In contrast, if the inherent friction on the joint system is properly compensated, the expected joint velocity versus interaction torque curve will exhibit a smaller interaction torque with an elliptical profile, as indicated by the solid line in Fig. 9. The elliptical profile of the curve is attributed to the effect of inertia on the system.

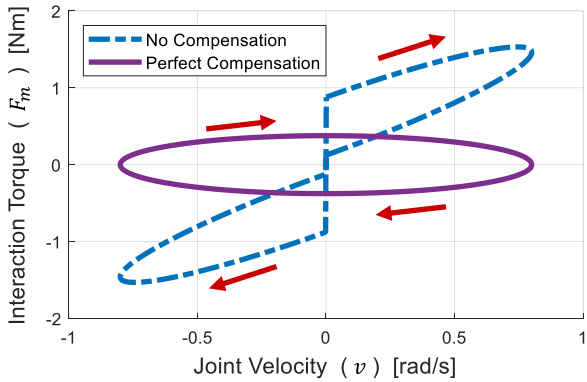

Fig. 9. Joint velocity versus interaction torque curve with the simulation of the friction acting on the mass. The dashed line indicates the curve with combined (Coulomb + viscous) friction. The solid line denotes the curve when friction is perfectly compensated.

The proposed friction compensation method to compensate for the combined friction was implemented on a single joint of a robot arm to demonstrate its efficacy. The velocity and measured interaction torque of the joint are recorded in Fig. 10(a), and the resulting net energy input in Fig. 10(b). As expected, the initial two cycles displayed an increase in energy because our approach requires at least two cycles to estimate and compensate for friction. When the operator changes his/her driving direction of the robot and the instance when the robot joint velocity reduces to zero, a transition moment between each energy cycle is detected.

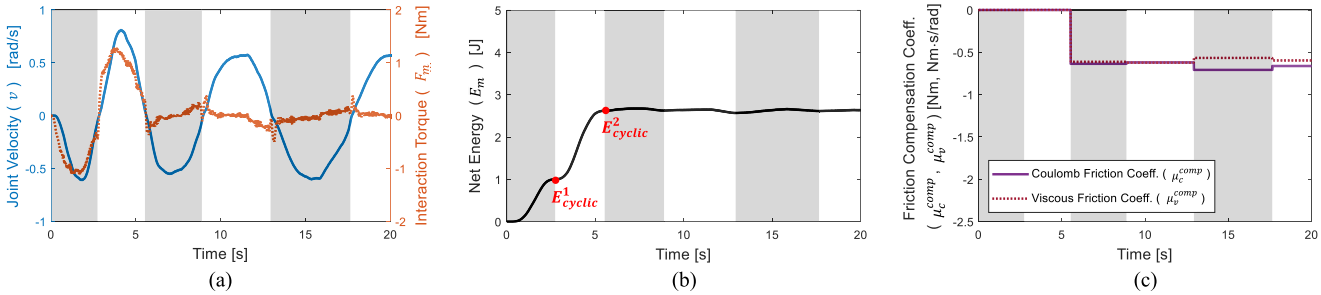

Fig. 10. Experimental data with proposed friction compensation method on a single joint of the robot arm. (a) Joint velocity and interaction torque. (b) Net energy input from the human operator to the robot joint. The energy increases within the initial two cycles but is maintained thereafter. (c) Viscous and Coulomb friction compensation coefficient estimated with the proposed friction compensation method.

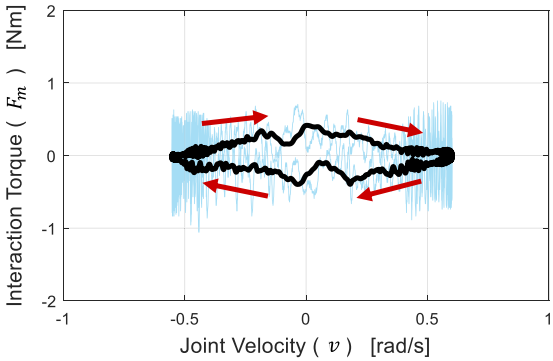

Fig. 11. Joint velocity versus interaction torque curve with raw (blue) and filtered (black) values.

This transition moment is indicated by a change in background color in the plots. The viscous and Coulomb friction coefficients are calculated at each transition instance based on the energy difference in the respective cycle, as illustrated in Fig. 10(c). These coefficients are then applied to compensate for the friction of the consecutive cycle. Once the friction compensation is activated, the friction compensation successfully maintains the net input energy in the vicinity of E^2_{cyclic}, which represents the resulting net energy input of the second cycle. Fig. 11 illustrates the joint velocity versus the interaction torque curve obtained using the proposed approach with the combined friction model. Notably, the maximum required interaction torque between the human operator and the robot joint drastically decreased from approximately 1.5 N·m to below 0.5 N·m compared to the case wherein no friction compensation torque was applied to the system, as shown in Fig. 8(c). Furthermore, the shape of the curve exhibited an elliptical profile, in contrast to the previous plot in which no friction compensation was applied. This behavior is similar to the simulation result depicted by the solid line in Fig. 9, where friction is perfectly compensated.

In summary, our proposed friction estimation and compensation method demonstrated its effectiveness in compensating the joint friction torque through experimental validation, as demonstrated by the net energy-input behavior during interaction with a human operator and the joint velocity versus interaction torque curve.

B. Extension to the Multi-DoF Robot Arm Interaction

In a previous single-DoF experiment, a human operator interacted with a robot by directly applying torque to a single joint. However, in multi-DoF interaction experiments, the human operator indirectly applies torque to the lower joint by indirect interaction through the end effector, instead of applying torque individually to each joint.

A straightforward extension of the single-DoF scheme to a multi-DoF scheme involves the individual application of a single-DoF scheme to each joint. However, this individual implementation causes an asynchronous update of the friction compensation coefficients at each joint, which may introduce a sudden disturbance torque into neighboring joints in the middle of the friction estimation. For example, if the friction coefficient of the upper joint is updated in synchronization with the zero velocity of the joint, the torque transmitted from the end effector to the lower level joints through this joint will suddenly be altered owing to the compensated friction torque. However, if this event occurs when the lower level joint is in the middle of the friction estimation cycle, the accumulated input energy at the lower joint is distorted, leading to improper friction estimation. Therefore, to synchronously update the friction compensation coefficient for each joint, we utilized the task space velocity of the robot arm end effector to define a cycle for a multi-DoF extension while monitoring the net energy input in the joint space. In addition, to achieve a synchronized update of the friction coefficients for all joints, the energy cycle update necessitates substantial movement across all joints. This guarantees the simultaneous update of all joint friction coefficients.

Our proposed friction compensation method effectively addresses the common challenges associated with using redundant robots, such as null space movement and singularities. By utilizing the robot as an impedance-type haptic device, human arm movements become the primary force driving the robot arm joints. As a result, when the robot arm's end effector is held stationary by the human operator, the joints naturally stop moving. Although active components such as gravity compensation and friction compensation torques could potentially induce null-space movements, the passivity controller applied to all joints makes such movements unlikely. Furthermore, the issue of singular motion, where joint space motion does not lead to task space motion, does not arise because the task space

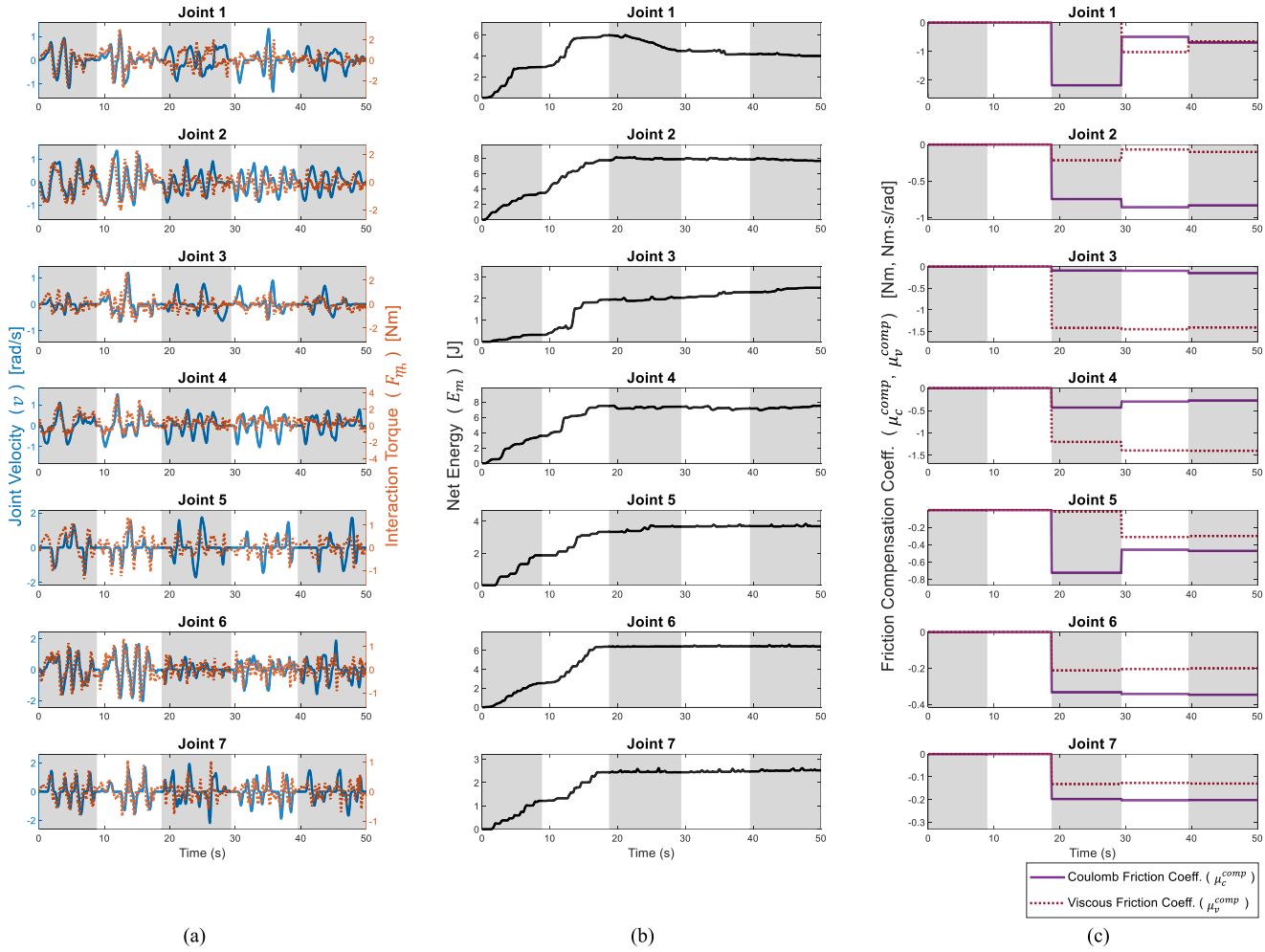

Fig. 12. Experimental data with proposed friction compensation approach extended to 7 joints of the robot arm. Each row depicts the experimental data of each joint and a change in background color indicates a change in energy cycle. (a) Velocities and torques of the robot joints interacting with human operator. (b) Net energy exchange between robot and human operator. (c) Estimated friction compensation coefficient of combined friction model.

motion of the human hand is the main driving force for the robot joints.

The proposed task-space cycle-detecting criterion was utilized to extend the friction compensation approach to a 7-DoF Franka Emika Panda robot (see Fig. 12), and the combined friction model is used for all joints. As observed in the single-DoF experiment, the energies of the joints initially increased because of the friction compensation approach, which required at least two cycles to estimate and compensate for friction [see Fig. 12(b)]. After the initial two cycles were detected based on the task-space velocities, the viscous and Coulomb friction coefficients for all the joints were calculated and synchronously applied to the system [see Fig. 12(c)]. The background color in the plots represents the change in energy cycles. As depicted in the energy plot Fig. 12(b), the cyclic energies of the joints stopped increasing and maintained their values for the remaining cycles, indicating effective compensation of the inherent friction in the system. Thus, our experimental results validate the ability of the proposed approach to effectively compensate for the intrinsic joint frictions of multi-DoF robotic systems.

In Fig. 12(c), the estimated friction coefficients for joint 1 and joint 5 experienced drastic change after the third cycle. This sudden change is likely due to the potential misestimation of our combined friction coefficient estimation approach when a small number of cycles is used for estimation, as discussed in the final paragraph of Section III. However, such drastic changes are typically not perceptible to the human operator, and the passivity controller in our friction compensator is designed to address any possible instability due to overcompensation.

C. Comparison With Other Friction Compensation Methods

This section presents the experiments conducted to evaluate and compare the performance of the proposed friction compensation approach with three different friction compensation methods. First, we compared our approach with the model-based friction estimation and compensation methods proposed in [13]. The primary rationale behind our selection of this study is that this is the only work that identifies the friction parameters of

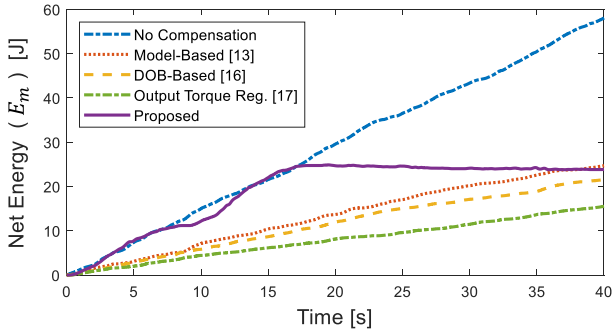

Fig. 13. Net energy exchange between robot and human operator with different friction compensation methods.

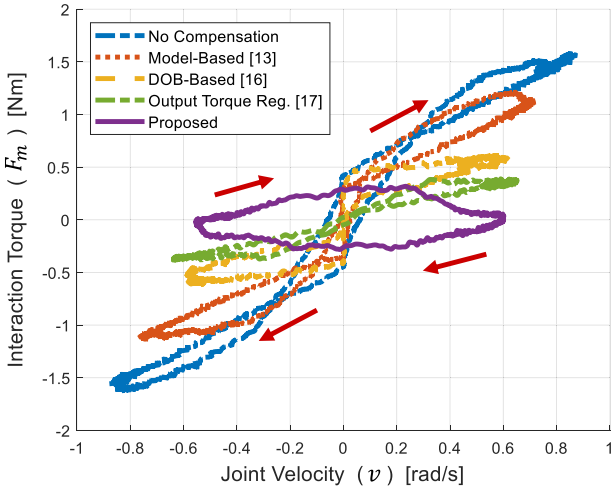

Fig. 14. Joint velocity versus interaction torque curve with different friction compensation methods. Stronger filters are applied for clear visualization.

a Franka Emika Panda robot arm that we utilize in our study. This method estimates the coefficients of the Lugre friction model [21] for the joints of the Franka Emika Panda robot arm using a penalty-based optimization method. The parameters identified in this study are directly applied to our system. Second, we compared our approach with the DOB-based method proposed in [16]. This method considers friction as a disturbance and estimates and compensates for it in real time. However, this method requires a dynamic model (motor inertia) and adjustable observer gains. In practice, motor inertia specifications are often undisclosed for commercially available robotic arms. Furthermore, even when these specifications are available, additional experimentation is required to fine-tune observer gains. In our experiments using the Franka Emika Panda robot, we experimentally adjusted the motor inertia values and observer gains for each joint to yield sufficient friction compensation while maintaining system stability. Finally, An output torque regulation method [17], which provides torque regulation in industrial collaborative robots with joint torque sensor is also added to the comparison. The key parameter in this method is desired motor inertia B_θ. Given that the robot used in [17] differs from the one in our experiments, we conducted additional tuning procedure to define minimum B_θ, while ensuring stable robot operation.

We conducted experiments for comparison in multi-DoF, including a model-based approach [13], a DOB-based approach [16], an output torque regulation method [17], and the proposed approach. The net energy inputs for each method, including the baseline case without compensation, are represented in Fig. 13. The net energy input profiles of the model-based, DOB-based, and output torque regulation approaches exhibited a continuously increasing behavior. The slopes of the energy profiles of these three methods showed reduction compared to the no compensation case, with the output torque regulation approach demonstrating the most gradual slope, and the model-based approach displaying the steepest slope. This observation indicates that the output torque regulation method compensated friction more accurately, surpassing the accuracy of both the DOB-based and model-based approaches. It also indicates that the DOB-based approach had more accurate friction compensation than the model-based approach. However, considering that the net energy input continues to exhibit a continuously increasing profile, the output torque regulation, DOB-based, and model-based methods tended to undercompensate the intrinsic joint friction.

In contrast, the proposed friction compensation method exhibits an initial rapid increase in energy owing to the delayed application of the friction compensation torque until the second energy cycle is detected. However, after the detection of the initial two energy cycles, the proposed method estimates and compensates for joint friction more accurately, resulting in the maintenance of the energy value. This sustained energy behavior demonstrates the method's precise estimation and compensation for intrinsic joint friction, surpassing the performance of other evaluated methods such as model-based, DOB-based, and output torque regulation approaches. These listed conventional methods depend on model information, which is typically inaccurate and requires fine-tuning of key parameters. In contrast, our energy-based method streamlines the process by reducing dependency on such uncertain and time-varying system parameters, thereby enhancing performance and adaptability. This fundamental shift toward an energy-centric approach not only achieves performance but also simplifies the process, marking a significant advancement in friction compensation strategies.

In addition, the joint velocity versus the interaction torque curve for each approach is presented in Fig. 14, including the no-compensation case as a baseline. Note that although we have collected data for all multi-DoF scenarios, we chose to present the results in joint space to highlight the efficacy of friction compensation. The plot indicates that the maximum interaction torque applied by the human operator decreases across various friction compensation approaches. Specifically, there is a reduction with the model-based approach, followed by a more pronounced decrease with the DOB-based method. Further reduction is noted when employing the output torque regulation approach. However, the joint velocity versus the interaction torque curves of these three methods still include the effects of viscous and Coulomb friction, similar to the case

without compensation illustrated in Fig. 9, indicating inadequate friction compensation. In contrast, the joint velocity versus the interaction torque curve of the proposed approach suggests that the characteristics of inherent viscous and Coulomb friction in the system are significantly reduced. These results demonstrate that the proposed approach outperforms other state-of-the-art friction compensation methods, thereby enabling human operators to interact with robots by using less interaction torque in the system.

VI. Conclusion

This study proposed a model-free energy-based method for compensating friction in industrial collaborative robots used as haptic displays. Our technique utilized the correlation between the input energy, stored energy, and energy lost through friction to adaptively estimate the time-varying friction coefficient. The principal concept that enabled this estimation without requiring model information was the transparent energy relationship between the net energy input and energy dissipated by friction when the stored energy equals zero. Moreover, the proposed method was assessed via simulation and demonstrated desirable performance with assured stability alongside TDPA. Furthermore, the efficacy of the proposed strategy was demonstrated by human–robot interaction experiments with a Franka Emika Panda robot utilizing both single-DoF and multi-DoF systems. The findings revealed that the proposed method outperformed other state-of-the-art friction compensation approaches, including model-, DOB-, and output torque regulation-based methods.

The proposed method allows for the estimation and compensation of time-varying friction in a robot manipulator during spontaneous movements by a human operator, without the need for predefined trajectories. However, it is important to acknowledge certain limitations of our approach. In scenarios where the human operator consistently applies force to the robot in a way that prevents the kinetic energy from reaching zero, our friction coefficient estimation method, which relies on defining an energy cycle, becomes inoperable. While this limitation exists in our approach, it is worth noting that such scenarios of continuous and uninterrupted force application are extremely rare in the context of pHRI, as most tasks involve sequences of intermittent stop-and-go movements. In addition, in a multi-DoF interaction scenario, there may be instances where the operator's movement does not involve any movement in specific joints for several cycles. While such situations are also uncommon, as pHRI rarely involves such repetitive constrained movements, they could lead to the friction coefficient not being updated due to the absence of energy cycles in those specific joints.

In future research, we aim to enhance the performance of our proposed friction compensation method by incorporating a more advanced friction model that includes nonlinear phenomena, such as the Stribeck effect and static friction. In addition, we plan to integrate this method with traditional approaches to improve the overall pHRI experience. For instance, by integrating our method with inertia reshaping techniques, we aim to provide a lighter feeling for the human operator during interacting with a robot. We also aim to research an adaptive method to determine the velocity initiation and termination thresholds to increase the portability of the proposed approach across different platforms. Furthermore, as this research stems from the idea of using robot arms as haptic devices, we intend to incorporate additional haptic control strategies to augment the performance of collaborative industrial robot-based haptic interactions.

References

[1] S. Knopp, M. Lorenz, L. Pelliccia, and P. Klimant, "Using industrial robots as haptic devices for VR-training," in *Proc. IEEE Conf. Virtual Reality 3D User Interfaces (VR)*, 2018, pp. 607–608.

[2] A. Hentout, M. Aouache, A. Maoudj, and I. Akli, "Human–robot interaction in industrial collaborative robotics: A literature review of the decade 2008–2017," *Adv. Robot.*, vol. 33, no. 15/16, pp. 764–799, 2019.

[3] A. Grau, M. Indri, L. Lo Bello, and T. Sauter, "Robots in industry: The past, present, and future of a growing collaboration with humans," *IEEE Ind. Electron. Mag.*, vol. 15, no. 1, pp. 50–61, Mar. 2021.

[4] A. Albu-Schäffer, S. Haddadin, A. Ott, A. Stemmer, T. Wimböck, and G. Hirzinger, "The DLR lightweight robot: Design and control concepts for robots in human environments," *Ind. Robot: Int. J.*, vol. 34, no. 5, pp. 376–385, 2007.

[5] P. Kremer et al., "Multimodal telepresent control of DLR's Rollin' JUSTIN," in *Proc. IEEE Int. Conf. Robot. Autom.*, 2009, pp. 1601–1602.

[6] M. Schwarz et al., "Robust immersive telepresence and mobile telemanipulation: Nimbro wins ana avatar xprize finals," in *Proc. IEEE-RAS 22nd Int. Conf. Humanoid Robots (Humanoids)*, 2023, pp. 1–8.

[7] A. Ajoudani, A. M. Zanchettin, S. Ivaldi, A. Albu-Schäffer, K. Kosuge, and O. Khatib, "Progress and prospects of the human–robot collaboration," *Auton. Robots*, vol. 42, pp. 957–975, 2018.

[8] H. Olsson, K. J. Åström, C. C. De Wit, M. Gäfvert, and P. Lischinsky, "Friction models and friction compensation," *Eur. J. Control*, vol. 4, no. 3, pp. 176–195, 1998.

[9] M. J. Kim, F. Beck, C. Ott, and A. Albu-Schäffer, "Model-free friction observers for flexible joint robots with torque measurements," *IEEE Trans. Robot.*, vol. 35, no. 6, pp. 1508–1515, Dec. 2019.

[10] W. Susanto, R. Babuška, F. Liefhebber, and T. van der Weiden, "Adaptive friction compensation: Application to a robotic manipulator," *IFAC Proc. Volumes*, vol. 41, no. 2, pp. 2020–2024, 2008.

[11] S. Huang, W. Liang, and K. K. Tan, "Intelligent friction compensation: A review," *IEEE/ASME Trans. Mechatronics*, vol. 24, no. 4, pp. 1763–1774, Aug. 2019.

[12] M. R. Kermani, R. V. Patel, and M. Moallem, "Friction identification and compensation in robotic manipulators," *IEEE Trans. Instrum. Meas.*, vol. 56, no. 6, pp. 2346–2353, Dec. 2007.

[13] C. Gaz, M. Cognetti, A. Oliva, P. Robuffo Giordano, and A. De Luca, "Dynamic identification of the Franka Emika Panda robot with retrieval of feasible parameters using penalty-based optimization," *IEEE Robot. Autom. Lett.*, vol. 4, no. 4, pp. 4147–4154, Oct. 2019.

[14] A. Wahrburg et al., "Modeling speed-, load-, and position-dependent friction effects in strain wave gears," in *Proc. IEEE Int. Conf. Robot. Autom.*, 2018, pp. 2095–2102.

[15] L. Simoni, M. Beschi, G. Legnani, and A. Visioli, "On the inclusion of temperature in the friction model of industrial robots," *IFAC-PapersOnLine*, vol. 50, no. 1, pp. 3482–3487, 2017.

[16] L. T. Le, "Passive friction compensation using a nonlinear disturbance observer for flexible joint robots with joint torque measurements," *J. Comput. Sci. Cybern.*, vol. 35, no. 1, pp. 85–103, 2019.

[17] A. Albu-Schäffer, C. Ott, and G. Hirzinger, "A unified passivity-based control framework for position, torque and impedance control of flexible joint robots," *Int. J. Robot. Res.*, vol. 26, no. 1, pp. 23–39, 2007.

[18] E. Franco, "IDA-PBC with adaptive friction compensation for underactuated mechanical systems," *Int. J. Control*, vol. 94, no. 4, pp. 860–870, 2021.

[19] R. Balachandran, "A stable and transparent framework for adaptive shared control of robots," Ph.D. dissertation, Technische Universitaet Muenchen, Munich, Germany, 2022. [Online]. Available: https://elib.dlr.de/188393/

[20] B. Hannaford and J.-H. Ryu, "Time-domain passivity control of haptic interfaces," *IEEE Trans. Robot. Autom.*, vol. 18, no. 1, pp. 1–10, Feb. 2002.

[21] K. Johanastrom and C. Canudas-De-Wit, "Revisiting the LuGre friction model," *IEEE Control Syst. Mag.*, vol. 28, no. 6, pp. 101–114, Dec. 2008.

Huseyin Tugcan Dinc (Graduate Student Member, IEEE) received the B.S. degree in mechatronics engineering from Erciyes University, Kayseri, Turkey, in 2016 and the M.S. degree from the Deggendorf Institute of Technology, Deggendorf, Germany, in 2020 with master's thesis conducted at German Aerospace Center (DLR), Institute of Robotics and Mechatronics, Wessling, Germany. He is currently working toward the Ph.D. degree in robotics with the Korea Advanced Institute of Science and Technology (KAIST), Daejeon, South Korea.

His current research interests include nonlinear control, particularly stable and safe interaction in haptics and teleoperation.

Joong-Ku Lee (Graduate Student Member, IEEE) received the B.S. degree in mechanical engineering in 2020 from Sungkyunkwan University, Suwon, South Korea, and the M.S. degree in robotics in 2022 from the Korea Advanced Institute of Science and Technology (KAIST), Daejeon, South Korea, where he is currently working toward the Ph.D. degree in civil and environmental engineering.

His research interests include telerobotics, haptics, and artificial intelligence.

Jee-Hwan Ryu (Senior Member, IEEE) received the B.S. degree from Inha University, Incheon, South Korea, in 1995, and the M.S. and Ph.D. degrees from the Korea Advanced Institute of Science and Technology, Daejeon, South Korea, in 1997 and 2002, respectively, all in mechanical engineering.

He is currently a Professor with the Department of Civil and Environmental Engineering, Korea Advanced Institute of Science and Technology. His research interests include haptics, telerobotics, teleoperation, exoskeletons, and autonomous vehicles